

Evidence for the droplet picture in the 3D $\pm J$ spin glass

Naomichi Hatano*

Center for Nonlinear Science and Theoretical Division

Los Alamos National Laboratory, Los Alamos, NM 87545 and

Department of Physics, Aoyama Gakuin University, Setagaya, Tokyo 157-8572, Japan

James E. Gubernatis

Center for Nonlinear Science and Theoretical Division

Los Alamos National Laboratory, Los Alamos, NM 87545

(Dated: December 2, 2024)

Abstract

A bivariate version of the multicanonical Monte Carlo method and its application to the simulation of the three-dimensional $\pm J$ Ising spin glass are described. We found the autocorrelation time associated with this particular multicanonical method was approximately proportional to the system volume, which is a great improvement over previous methods applied to spin-glass simulations. The principal advantage of this version of the multicanonical method however was its ability to access information predictive of low-temperature behavior. At low temperatures we found results on the three-dimensional $\pm J$ Ising spin glass consistent with the droplet picture: the order-parameter distribution function $P(q)$ converged to two delta-function peaks, and the Binder parameter approached unity as the system size was increased. We also discuss the structure of the ground-state degeneracy, introducing the concept of zero-energy droplets. The size distribution of the zero-energy droplets was found to produce the two delta-function peaks of $P(q)$.

PACS numbers: 75.10.Nr, 75.50.Lk, 05.10.Ln

*hatano@phys.aoyama.ac.jp; <http://www.phys.aoyama.ac.jp/~hatano>

I. INTRODUCTION

Although a quarter century has passed since the pioneering work on spin glasses by Edwards and Anderson [1], many fundamental problems remain unsolved even for the simplest models of spin glasses [2]. In the present paper, we report the results of our recent Monte Carlo simulations of the three-dimensional $\pm J$ Ising spin glass, focusing on the nature of the low-temperature phase [3, 4]. We believe we have found important evidence of ground-state properties consistent with the droplet picture of Fisher and Huse [5, 6].

The spin-glass state is characterized by randomly quenched exchange interactions with frustration. Often systems exhibiting this state are modeled by the $\pm J$ Ising model. In three dimensions this model is defined by the Hamiltonian [1]

$$\mathcal{H} \equiv - \sum_{\langle i,j \rangle} J_{ij} \sigma_i \sigma_j. \quad (1)$$

where the Ising spins σ_i fluctuate thermodynamically, while each exchange interaction J_{ij} is quenched to $\pm J$ randomly. The summation runs over the nearest-neighbor pair of sites on a cubic lattice.

The frustration of local spin configurations by the exchange interactions generate many local minima in the free energy landscape, each minimum representing a seemingly random configuration of the spins. At low temperatures, the spins, however, may freeze into such a configuration, and this freezing is the essence of the spin-glass “order.” Because of the nature of this order, equilibration of spin glasses in simulations and experiments is often very hard. After a few decades of research, unresolved issues on equilibrium properties of spin glasses remain.

It is becoming increasingly accepted that the $\pm J$ model has a finite-temperature spin-glass phase transition in three dimensions, particularly after two recent independent Monte Carlo studies [7, 8]. The nature of the low-temperature phase, however, is still controversial. The controversy is between the mean-field and droplet pictures. The mean-field picture maintains the existence of an infinite number of global minima of the free energy in the low-temperature phase. The condition is called replica symmetry breaking [9]. The breaking of this symmetry is rigorously true for the mean-field (Sherrington-Kirkpatrick) solution of the $\pm J$ Ising model [10, 11]. The question is whether it is also found in finite-dimensional non-mean-field models. The droplet picture [5, 6], on the other hand, asserts that the free-energy

landscape has only two global minima that are connected through spin inversion symmetry. According to the droplet picture, the nature of the spin-glass transition is less exotic in three dimensions than in the mean-field model.

The difference between the two pictures becomes quantitative when we use the order parameter of the spin-glass phase, namely the overlap order parameter [1]. To define this order parameter, we replicate the random exchange interactions in (1) and change the Hamiltonian to

$$\mathcal{H} \equiv - \sum_{\alpha=1,2} \sum_{\langle i,j \rangle} J_{ij} \sigma_i^{(\alpha)} \sigma_j^{(\alpha)}, \quad (2)$$

where the superscript of the spin variables indicates each replica of the system. The overlap order parameter is then defined as the Hamming distance between two spin configurations of the replicas [1]:

$$q = \frac{1}{L^d} \sum_{i=1}^{L^d} \sigma_i^{(1)} \sigma_i^{(2)}. \quad (3)$$

Here L is the linear size of the system and d is the dimensionality, which is three throughout the paper.

The spins of one replica and those of the other are thermodynamically independent. Still they can be correlated because of the common random exchange interactions. In the high-temperature limit, the spin configurations are uncorrelated, and hence the overlap order parameter tends to zero as $L^{-d/2}$. In the low-temperature limit, on the other hand, the spin configurations are frozen into energy minima, and hence the overlap order parameter can have a finite value.

In the droplet picture, the overlap order parameter at low temperatures and in the thermodynamic limit can take only two values equal and opposite to each other, as the frozen spin configuration of one replica is either macroscopically identical to the configuration of the other replica or to its inverted configuration. (Note, however, that the identity needs only to be macroscopic; the configurations can differ locally.) Hence the overlap order parameter q takes one of the two values with an equal probability. In the mean-field picture, on the other hand, the overlap order parameter can take various values. Because of the many free-energy minima, the frozen spin configurations of the two replicas can be very different.

More explicitly, we define the order-parameter distribution as

$$P(q) \equiv \left[\frac{1}{\mathcal{Z}} \sum_E D(E, q) e^{-\beta E} \right]_{\text{av.}}, \quad (4)$$

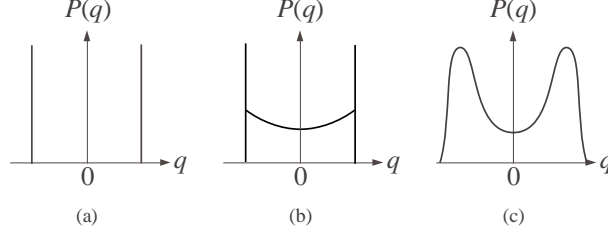


FIG. 1: The functional form of the order-parameter distribution $P(q)$ in the low-temperature phase: (a) According to the droplet picture; (b) According to the mean-field picture; (c) For finite-sized systems.

where the partition function is given by

$$\mathcal{Z} \equiv \sum_{\{\sigma\}} e^{-\beta E(\{\sigma\})} = \sum_q \sum_E D(E, q) e^{-\beta E}. \quad (5)$$

In these two equations $D(E, q)$ is the normalized density of states with respect to the energy E and the overlap order parameter q . The energy in Eqs. (4) and (5) and hereafter (including the Monte Carlo simulation) is the energy of the replica Hamiltonian (2). The square brackets in Eq. (4) denote the random average over various samples $\{J_{ij}\}$. Physical quantities that are functions of q only are calculated as

$$[\langle f(q) \rangle]_{\text{av.}} = \sum_q f(q) P(q), \quad (6)$$

where the angular brackets denote the thermodynamic average; *e.g.*, the spin-glass susceptibility

$$\chi_{\text{sg}} = L^d \beta^2 [\langle q^2 \rangle - \langle q \rangle^2]_{\text{av.}} \quad (7)$$

and the Binder parameter

$$g_{\text{sg}}(T, L) \equiv \frac{3}{2} \left(1 - \frac{[\langle q^4 \rangle]_{\text{av.}}}{3 [\langle q^2 \rangle]_{\text{av.}}^2} \right). \quad (8)$$

The droplet picture and the mean-field pictures have the functional forms for $P(q)$ as shown in Fig. 1. In the droplet picture, the order-parameter distribution in the thermodynamic limit has two delta-function peaks, indicating two possible thermodynamic states (Fig. 1a). In the mean-field picture the order-parameter distribution has a continuous part between those peaks (Fig. 1b).

In practice, we can only simulate finite systems for which the order-parameter distribution looks as Fig. 1c. We need to see whether the distribution in Fig. 1c converges to Fig. 1a or Fig. 1b as $L \rightarrow \infty$. In particular, the component $P(0)$ makes a clear distinction between the two pictures:

$$\lim_{L \rightarrow \infty} P(0) \begin{cases} = 0 & \text{droplet picture,} \\ > 0 & \text{mean-field picture.} \end{cases} \quad (9)$$

While some simulations appear to support infinite degeneracy [12, 13, 14], others do not [15, 16, 17], and a recent analytic treatment argues against it [18, 19]. We note that the droplet picture is a theory concerning the *zero*-temperature fixed point, while most studies suggesting the validity of the mean-field picture are based on numerical estimates of $P(0)$ at T only as low as $0.7T_c$, where the glass transition temperature T_c is approximately 1.0. If the droplet picture is correct, it should at least be seen at temperatures lower than $0.7T_c$, the closer to $T = 0$ the better. Unfortunately, the slow dynamics of spin glasses has hindered numerical simulations from exploring the vicinity of the zero-temperature fixed point. We comment that a recent numerical study [20] demonstrated that results of the Migdal-Kadanoff approximation appear to support the mean-field picture near and below the glass transition temperature, but eventually support the droplet picture as $T \rightarrow 0$. Uncertainty, however, remains because the Migdal-Kadanoff approximation favors the droplet picture, even for the mean-field model [21, 22].

In the present study, we reduced the difficulty of the slow dynamics significantly by using a bivariate multicanonical Monte Carlo method. Multicanonical simulations produce the density of states as output, from which we can in principle calculate expectation values at any temperatures. Our estimation of $P(0)$ at low temperatures and as a function of lattice size suggests the droplet picture. We will discuss this result more fully in the next section. Details of the multicanonical Monte Carlo method are given in Appendix A.

An important issue is the correspondence between theories and experiments of spin glasses. As was stressed above, it generally takes a very long time to equilibrate experimental samples, and many experiments in fact can only explore the nonequilibrium behavior of spin glasses. The importance of understanding the nature of the low-temperature equilibrium states is linked to many different topics about the behavior of complex systems beyond the specific example of spin glasses [9] (*e.g.*, vortex glass, Bose glass, neural networks, etc.), and hence worth resolving. We also note the growing number of experimental efforts to accel-

erate the equilibration process (*e.g.*, using quantum fluctuations from transverse magnetic fields [23]).

We present our Monte Carlo results in Sect. II. The order-parameter distribution function $P(q)$ exhibits a predicted feature of the droplet picture of the low-temperature phase: $P(0)$ decreases at $T = 0.3$ as the system size is increased. The low-temperature behavior of the Binder parameter also suggests the droplet picture. In Sect. III we discuss further implications of our results for the ground-state degeneracy. Quantities characterizing the ground-state degeneracy again behave as the droplet picture predicts. We discuss possible reasons for previous simulations finding mean-field-like results in the last section. In Appendix A, we describe our simulation method, namely a bivariate multicanonical Monte Carlo method. Mono-variate multicanonical methods [24, 25] have been applied to spin glasses before [26, 27, 28]; we found, however, that by using a bivariate version we could reduce the correlation time of the simulation significantly. We show that the autocorrelation time is approximately proportional to the system size. Because the output of multicanonical simulations is the density of states, we can access any temperature in principle. In particular we explored the low-temperature region that has been hard to access by other Monte Carlo methods.

II. NUMERICAL RESULTS

We have carried out a bivariate multicanonical Monte Carlo simulation of the systems of size $L = 4$ (1904 samples), $L = 6$ (2843 samples), $L = 8$ (1015 samples), and $L = 10$ (1111 samples). The simulation method directly returns the density of states, a temperature independent quantity. During the simulation, the concept of a fixed temperature has little direct meaning. The method facilitates movement of the simulation across the rugged free energy landscape. Thermal equilibration at a fixed temperature thus is not a relevant concern. We will describe the details of the computational method in Appendix. A.

A. Order-parameter distribution

The output of the bivariate multicanonical method is the density of states $D(E, q)$. From it we straightforwardly calculated the order-parameter distribution $P(q)$, following Eq. (4).

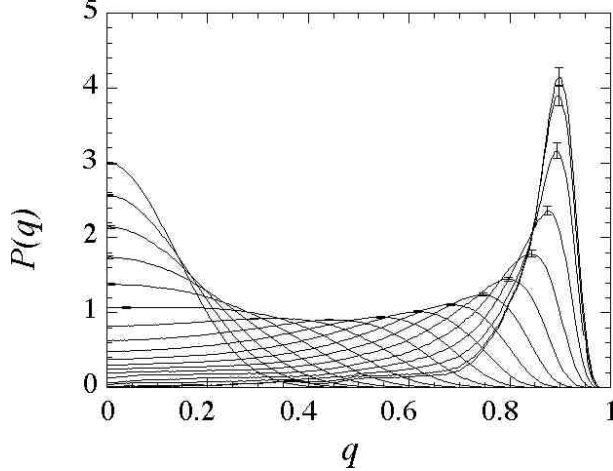
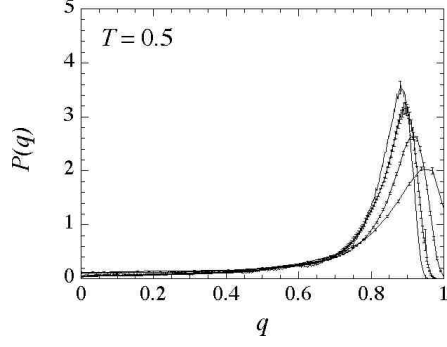


FIG. 2: The temperature dependence of the order-parameter distribution $P(q)$ for $L = 8$. The curves with the peak positions ordered from right to left correspond to $T = 0.3, 0.4, 0.5, \dots, 2.0$. The statistical errors are indicated only at each peak position. We plotted only for $0 \leq q \leq 1$, assuming the symmetry $P(-q) = P(q)$.

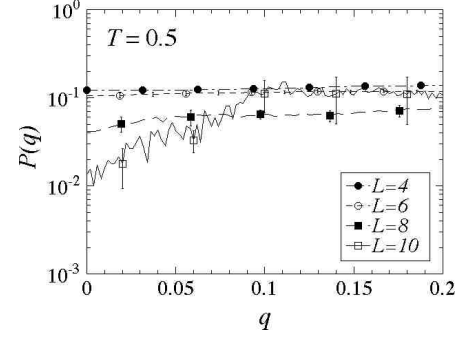
Figure 2 shows the temperature dependence of $P(q)$ for $L = 8$. The function is close to a Gaussian distribution at high temperatures and has a double-peak structure at low temperatures.

The results for $T = 0.3, 0.4$, and 0.5 are shown in Fig. 3 for several values of L . We clearly see the decreasing tendency of $P(0)$ as $L \rightarrow \infty$, which is the behavior predicted from the droplet picture. For $T \geq 0.7$, on the other hand, $P(0)$ does not show this tendency (Fig. 4). On the contrary, $P(0)$ appears to converge to a finite value. This behavior spuriously supports the mean-field picture.

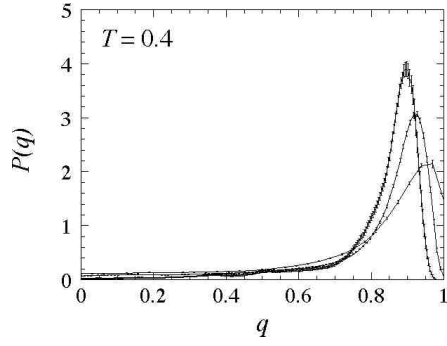
No matter which picture is correct, we know from the scaling ansatz that at the critical point $T = T_c \sim 1$, $P(0)$ should increase as $L \rightarrow \infty$. On the other hand, the droplet picture claims that $P(0)$ decreases, but perhaps only at very low temperatures. It is then reasonable to assume that if the droplet picture is correct, $P(0)$ appears independent of L over a range of the temperature around $T \sim \frac{1}{2}T_c$. This scenario is explicitly shown in Fig. 5. The same scenario was also predicted from Migdal-Kadanoff approximation [20]. We thus suggest that most previous Monte Carlo studies, claiming to see the mean-field picture, based their conclusions on their results for T only as low as 0.7 , and while they saw evidence consistent with mean-field picture, they missed the droplet picture which only appears at much lower



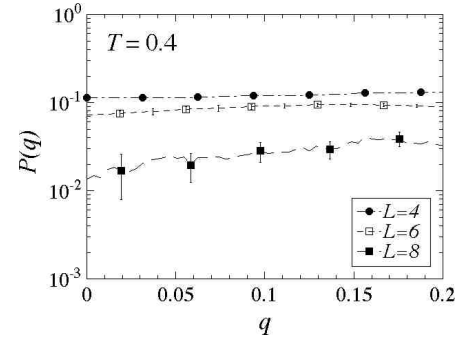
(a)



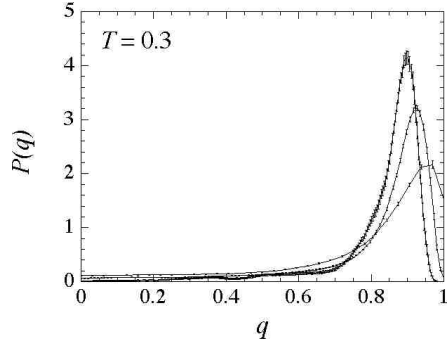
(b)



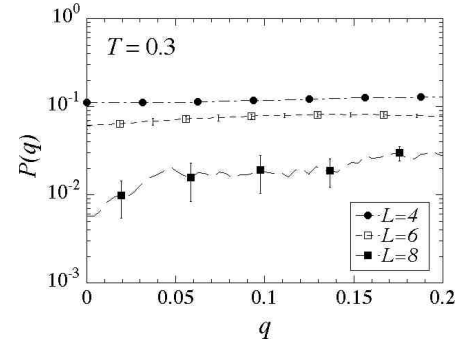
(c)



(d)

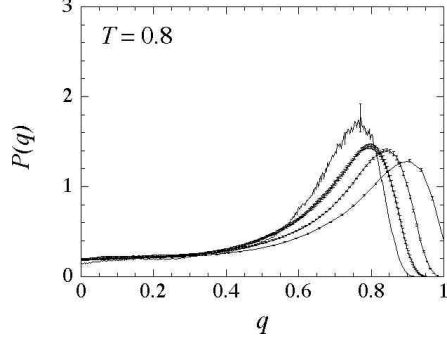


(e)

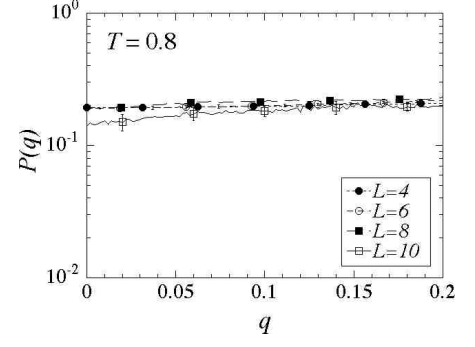


(f)

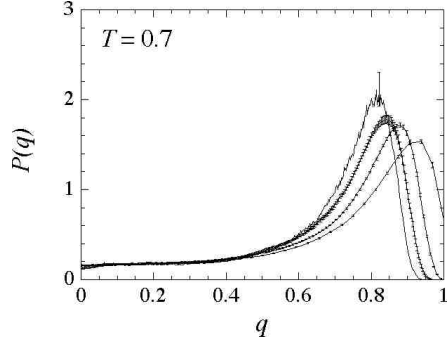
FIG. 3: The size dependence of the order-parameter distribution $P(q)$. (a) A linear plot for $T = 0.5$ and for $L = 4, 6, 8$, and 10 . The peak position moves left as the system size is increased. Because the data points are very dense for $L = 10$, the error bar is shown only at the peak, where the statistical error is the largest. (b) A semi-logarithmic plot for $T = 0.5$. The error bars are shown only for a part of the data points. (c) A linear plot for $T = 0.4$ and for $L = 4, 6$, and 8 . The peak position moves left as the system size is increased. (d) A semi-logarithmic plot for $T = 0.4$. The error bars are shown only for a part of the data points. (e) A linear plot for $T = 0.3$ and for $L = 4, 6$, and 8 . The peak position moves left as the system size is increased. (f) A semi-logarithmic plot for $T = 0.3$. The error bars are shown only for a part of the data points.



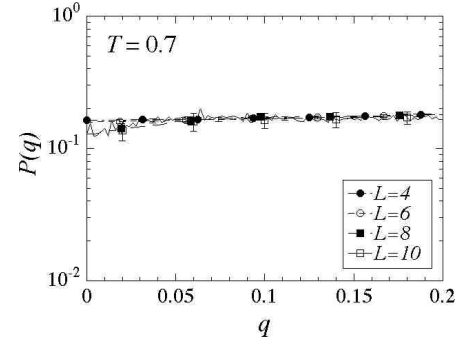
(a)



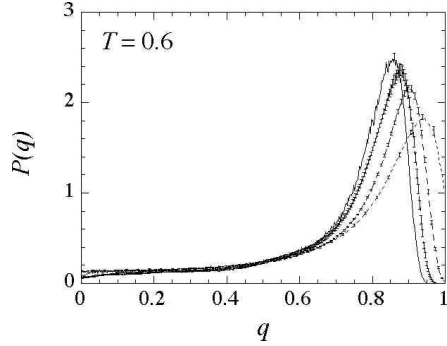
(b)



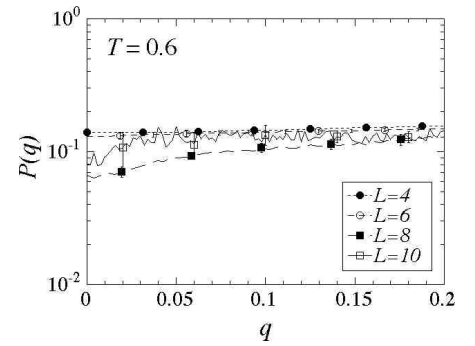
(c)



(d)



(e)



(f)

FIG. 4: The size dependence of the order-parameter distribution $P(q)$. (a) A linear plot for $T = 0.8$ and $L = 4, 6, 8$, and 10. The peak position moves left as the system size is increased. Because the data points are very dense for $L = 10$, the error bar is shown only at the peak, where the statistical error is the largest. (b) A semi-logarithmic plot for $T = 0.8$. The error bars are shown only for a part of the data points. (c) A linear plot for $T = 0.7$ and for $L = 4, 6, 8$, and 10. The peak position moves left as the system size is increased. For $L = 10$, the error bar is shown only at the peak. (d) A semi-logarithmic plot for $T = 0.7$. The error bars are shown only for a part of the data points. (e) A linear plot for $T = 0.6$ and for $L = 4, 6, 8$, and 10. The peak position moves left as the system size is increased. For $L = 10$, the error bar is shown only at the peak. (f) A semi-logarithmic plot for $T = 0.6$. The error bars are shown only for a part of the data points.

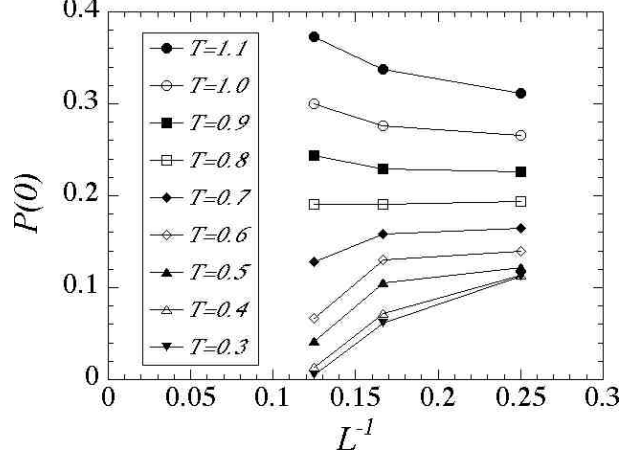


FIG. 5: The size dependence of $P(0)$ for $T = 1.1, 1.0, 0.9, \dots, 0.3$. The data for $T = 0.8$ *appear* to be independent of L , but the data at lower temperatures reveal features of the droplet picture.

temperatures.

B. Binder parameter

The Binder parameter for spin glasses g_{sg} is defined by Eq. (8). This parameter is essentially the kurtosis of the order-parameter distribution $P(q)$. Because of the dimensionless combination of the second moment and the fourth moment, the Binder parameter (except for effects due to correction to scaling) is expected to be independent of the system size at fixed points, *i.e.*, $T = 0$, $T = T_c$, and $T \rightarrow \infty$. For conventional phase transitions such as ferromagnetic transitions, the temperature dependence of the Binder parameter for various system sizes has a crossing point at the critical temperature. At the high-temperature fixed point $T \rightarrow \infty$, the order-parameter distribution $P(q)$ should be Gaussian. Hence we should have

$$\int q^4 P(q) dq = 3 \left(\int q^2 P(q) dq \right)^2, \quad (10)$$

or

$$\left[\langle q^4 \rangle \right]_{\text{av.}} = 3 \left[\langle q^2 \rangle \right]_{\text{av.}}^2. \quad (11)$$

Thus the fixed-point value of the Binder parameter is zero for $T \rightarrow \infty$, *i.e.*, $g_{\text{sg}}(\infty, L) = 0$. In the high-temperature phase, the Binder parameter $g_{\text{sg}}(T, L)$ is renormalized to zero from above as $L \rightarrow \infty$. At the low-temperature fixed point, on the other hand, if the order

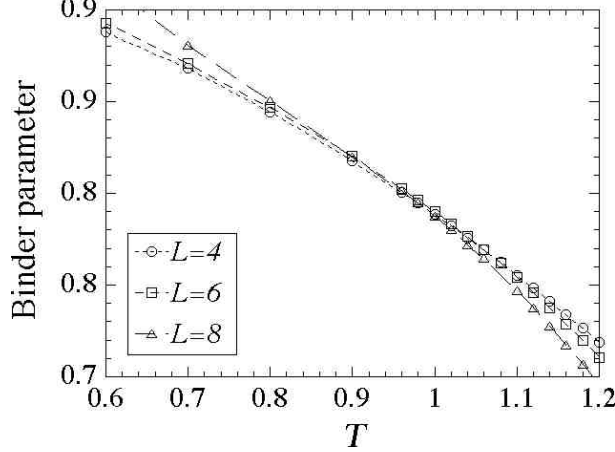


FIG. 6: The temperature dependence of the Binder parameter $g(T, L)$ for $L = 4, 6$, and 8 . The statistical errors are comparable to the symbol size.

parameter takes only two values $\pm q_0$, as in the thermodynamic limit of usual ferromagnets, we have

$$\left[\langle q^4 \rangle \right]_{\text{av.}} = \left[\langle q^2 \rangle \right]_{\text{av.}}^2 = q_0^4 \quad (12)$$

and hence the fixed-point value of the Binder parameter should be unity: $g_{\text{sg}}(0, L) = 1$. In the low-temperature phase, the Binder parameter $g_{\text{sg}}(T, L)$ should be renormalized to unity from below as $L \rightarrow \infty$. At $T = T_c$, the Binder parameter $g_{\text{sg}}(T_c, L)$ is expected to have a nontrivial universal value between zero and unity. Thus the crossing point of $g_{\text{sg}}(T, L)$ should give the critical temperature T_c .

Our Monte Carlo simulation found the crossing point of the Binder parameter as shown in Fig. 6. The crossing point should be in the region $0.8 \geq T_c \geq 1.1$. For the moment, because of strong corrections to scaling, it is difficult for us to carry out sophisticated scaling analysis and obtain a more accurate estimate,. Previous studies [7, 8] claim $T_c \simeq 1.1$.

Further evidence for the droplet picture is found in the low-temperature behavior of the Binder parameter (Fig. 7). This result strongly suggests that the Binder parameter tends to unity as $T \rightarrow 0$ and $L \rightarrow \infty$. As explained above, the $T = 0$ Binder parameter in the thermodynamic limit will be unity if the order parameter takes only two values. This behavior is consistent with the droplet as illustrated in Fig. 1a. On the other hand, according to the mean-field picture as illustrated in Fig. 1b, the Binder parameter is less than unity even at $T = 0$ and $L \rightarrow \infty$. Our Monte Carlo result clearly supports the droplet picture

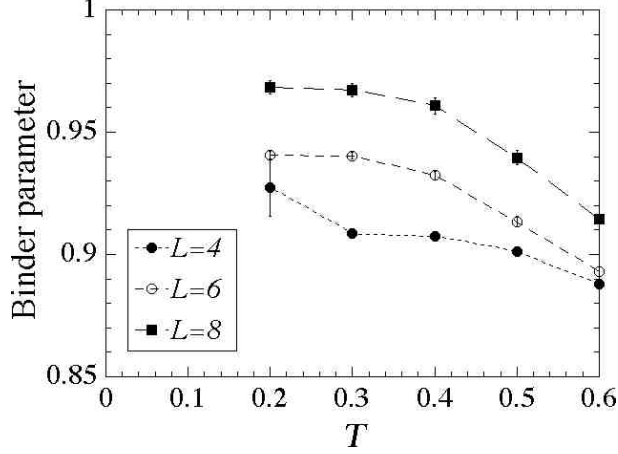


FIG. 7: The temperature dependence of the Binder parameter $g(T, L)$ for $L = 4, 6$, and 8 .

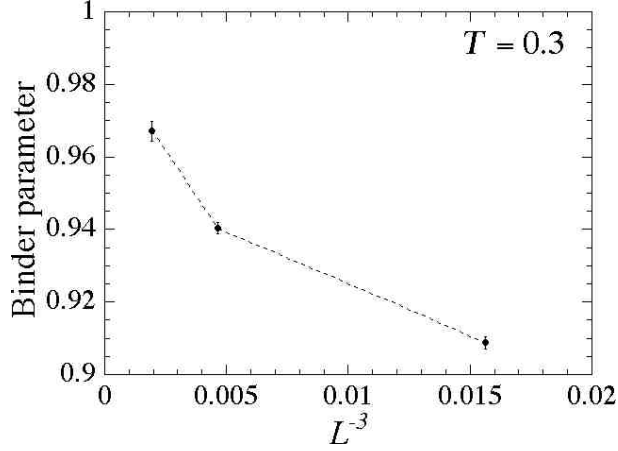


FIG. 8: The size dependence of the Binder parameter at $T = 0.3$. The Binder parameter is approaching unity rapidly.

(see Fig. 8).

C. Residual entropy

We calculated the entropy density from the difference between the energy and the free energy, *i.e.*

$$s = \frac{[\langle E \rangle]_{\text{av.}} - F}{NT}, \quad (13)$$

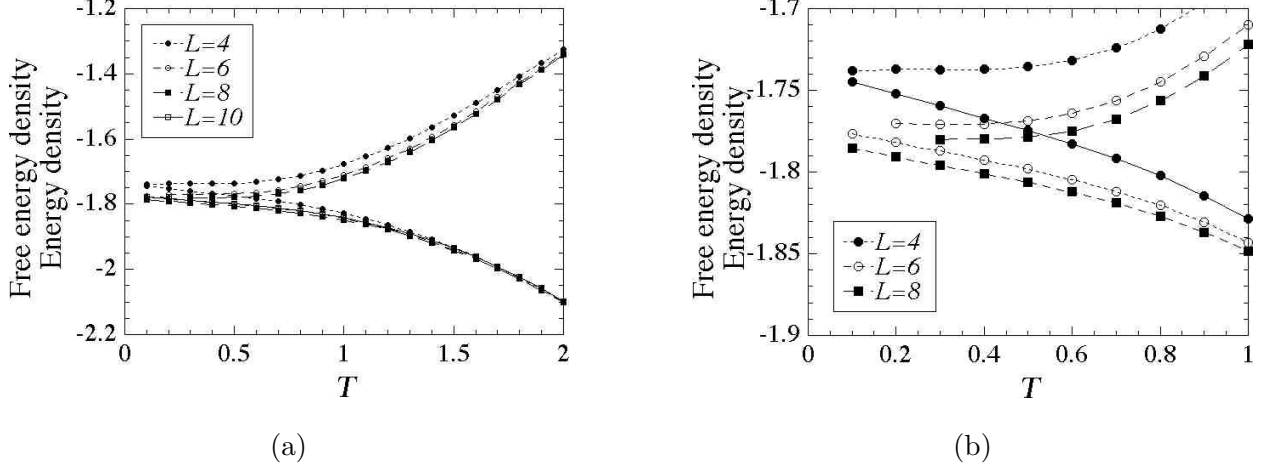


FIG. 9: The temperature dependence of the energy density and the free-energy density. (b) is an enhanced view of (a). The statistical errors are smaller or comparable to the symbol size.

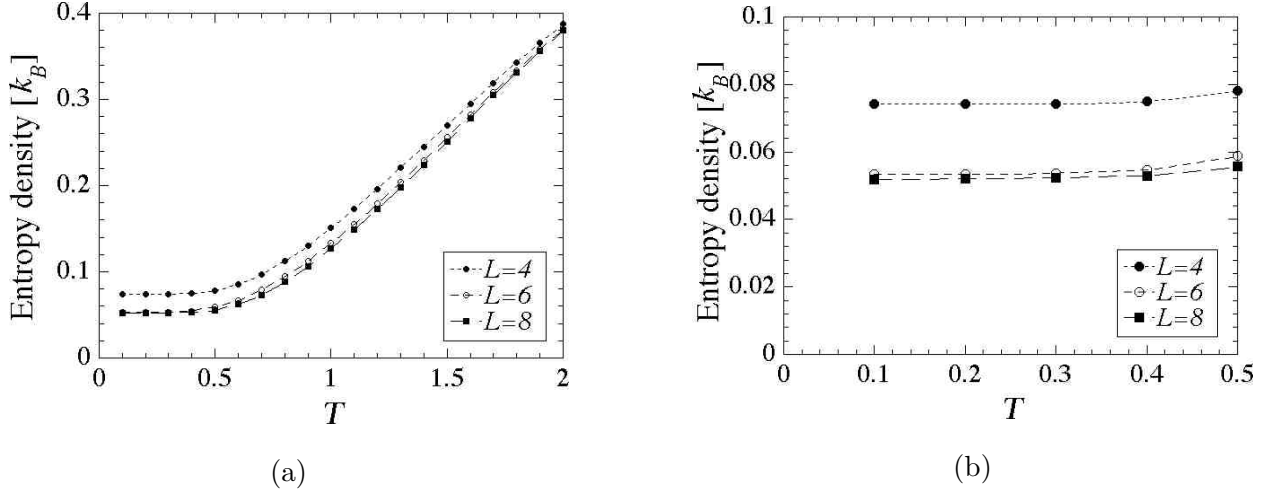


FIG. 10: The temperature dependence of the entropy density. (b) is an enhanced view of (a). The statistical errors are smaller or comparable to the symbol size.

where F is the free energy calculated from the Monte Carlo output $D(E, q)$ via

$$F = -\frac{1}{\beta} \log Z = -\frac{1}{\beta} \log \left(\sum_{E, q} D(E, q) e^{-\beta E} \right). \quad (14)$$

Figure 9 shows the energy and free-energy densities. The difference between them is shown in Fig. 10. It is clear that at $T = 0.1$ the estimates of the entropy are virtually the residual entropy at $T = 0$. The residual entropy is plotted in Fig. 11, and it seems finite in the thermodynamic limit. Hartmann [29] obtained a similar estimate $s(T = 0) = 0.051(3)k_B$ from a ground-state search on systems up to $L = 8$.

Although Hartmann [29] used the existence of the residual entropy as evidence for the

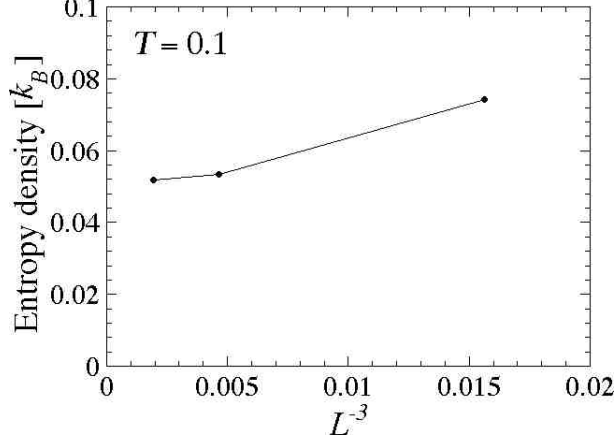


FIG. 11: The size dependence of the residual entropy. The statistical errors are smaller or comparable to the symbol size.

mean-field picture, its existence is on the contrary entirely consistent with the droplet picture. The degeneracy of the ground states predicted by the droplet and mean-field pictures is the degeneracy of thermodynamic (macroscopic) states, while the residual entropy comes from the degeneracy of microscopic states. The distinction is important to note.

Because the energy of the $\pm J$ model is discrete, there is an inevitable degeneracy of the ground states. The issue is whether the degeneracy calculated arises from these microscopically degenerate states or from many macroscopically different states. To make the distinction, we consider a toy model in which we quench the exchange interactions into a periodic configuration with a unit cell of linear size l . This model has a ground state with a periodic spin configuration. We will assume, however, that every unit cell has one connected cluster of spins such that the spin inversion of the cluster does not change the ground-state energy (See Fig. 12). We refer to such spin clusters as “zero-energy droplets.” The number of such droplets in a system of linear size L is $N_{\text{zed}} = (L/l)^d$, where d is the dimensionality. The degeneracy of the ground-state energy is $2^{N_{\text{zed}}}$. Therefore, the residual entropy density of the toy model takes a finite value

$$s_{\text{toy}}(T = 0) = L^{-d} \times k_B \ln(2^{N_{\text{zed}}}) = k_B l^{-d} \ln 2. \quad (15)$$

This toy model, on the other hand, produces a $P(q)$ of the form predicted by the droplet picture: Consider two replicas of the toy model. Without loss of generality, we can fix the spin configuration of one replica and calculate contributions from different spin configura-

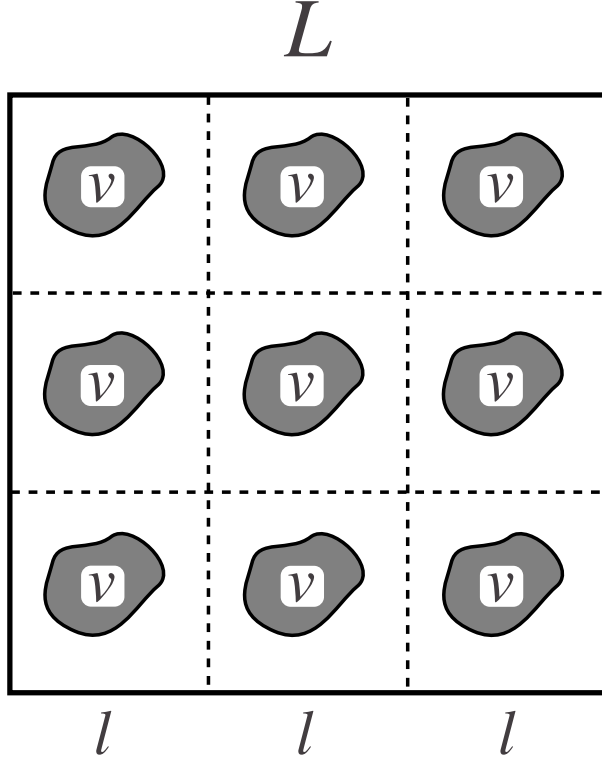


FIG. 12: Toy model with a finite residual entropy density and delta-function peaks in $P(q)$. In the figure, L is the linear size of the whole system, l is the size of the unit cell, and v is the volume of a zero-energy droplet.

tions of the other replica. The distribution of the order parameter is given by

$$\begin{aligned}
 |q| = 1 & \quad \text{with the probability } 2^{-N_{\text{zed}}}, \\
 |q| = 1 - 2v/L^d & \quad \text{with the probability } 2^{-N_{\text{zed}}} \times N_{\text{zed}}, \\
 |q| = 1 - 4v/L^d & \quad \text{with the probability } 2^{-N_{\text{zed}}} \times \frac{1}{2}N_{\text{zed}}(N_{\text{zed}} - 1), \\
 \dots & \\
 |q| = 1 - 2nv/L^d & \quad \text{with the probability } 2^{-N_{\text{zed}}} \times \binom{N_{\text{zed}}}{n} \\
 \dots, &
 \end{aligned} \tag{16}$$

where v is the volume of each zero-energy droplet. In the thermodynamic limit $L \rightarrow \infty$ or equivalently $N_{\text{zed}} \rightarrow \infty$, the probability for $n = N_{\text{zed}}/2$ overwhelms and hence $P(q)$ converges to a delta-function peak at

$$q = 1 - \frac{N_{\text{zed}}}{2} 2v/L^d = 1 - \frac{v}{l^d}. \tag{17}$$

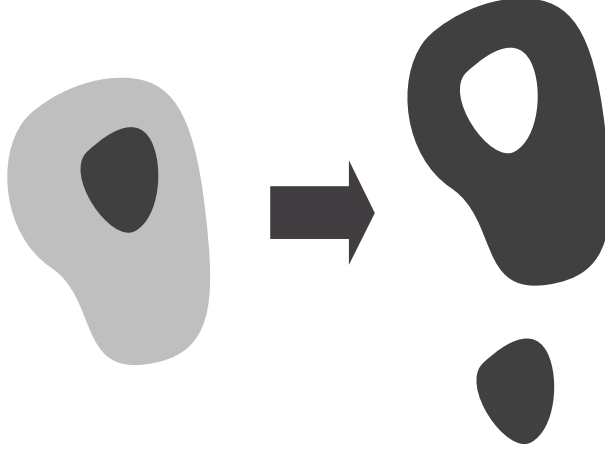


FIG. 13: If a zero-energy droplet contains another zero-energy droplet as shown on the left, we define the volumes of the two droplets as shown on the right.

and a second delta-function peak at $-q$.

III. GROUND-STATE DEGENERACY OF THE $\pm J$ MODEL

The toy model introduced at the end of the last section illustrates the essence of the droplet picture for the $\pm J$ model. It is easily converted to a more realistic argument for the ground-state degeneracy of the $\pm J$ model: Suppose the $\pm J$ model of linear size L has $N_{\text{zed}}(L)$ number of zero-energy droplets, where a zero-energy droplet is a cluster of spins whose inversion does not change the energy of an arbitrarily chosen ground-state spin configuration. The difference between this and the toy model is the zero-energy droplets of the $\pm J$ model having unequally-sized volumes v_i ($i = 1, 2, 3, \dots, N_{\text{zed}}(L)$). In defining the volume of zero-energy droplets, we always take the minimal volume; for example, if a zero-energy droplet contains another zero-energy droplet, we decompose them into two droplets shown in Fig. 13. In addition, the possible maximum volume of the zero-energy droplet is $L^d/2$: if there is a zero-energy droplet larger than the half of the system, we re-define the original ground-state spin configuration by flipping the largest zero-energy droplet.

The ground-state degeneracy is $2^{N_{\text{zed}}(L)}$, and hence the residual entropy density is given by

$$s(T = 0; L) = L^{-d} k_B \ln \left(2^{N_{\text{zed}}(L)} \right) = L^{-d} N_{\text{zed}}(L) k_B \ln 2. \quad (18)$$

We now define the distribution of the zero-energy droplets as $n_{\text{zed}}(v)$ so we have

$$N_{\text{zed}}(L) = L^d \int_1^{L^d/2} n_{\text{zed}}(v) dv. \quad (19)$$

Equation (18) is rewritten as

$$s(T=0; L) = k_B \ln 2 \times \int_1^{L^d/2} n_{\text{zed}}(v) dv. \quad (20)$$

Next, we consider the ground-state value of $\langle |q| \rangle$, and again we fix the spin configuration of one replica to the original ground-state spin configuration. Various contributions come from the spin configurations of the other replicas with some of the zero-energy droplets flipped. We extend Eq. (16) and obtain

$$\begin{aligned} |q| &= 1 && \text{with the probability } 2^{-N_{\text{zed}}}, \\ |q| &= 1 - 2v_i/L^d && \text{with the probability } 2^{-N_{\text{zed}}} \text{ for } i = 1, 2, \dots, N_{\text{zed}}, \\ |q| &= 1 - 2(v_i + v_j)/L^d && \text{with the probability } 2^{-N_{\text{zed}}} \text{ for } i, j = 1, 2, \dots, N_{\text{zed}} \text{ with } i < j, \\ &\dots && \\ |q| &= 1 - (2/L^d) \sum_{m=1}^n v_{i_m} && \text{with the probability } 2^{-N_{\text{zed}}} \\ &&& \text{for } i_1, i_2, \dots, i_n = 1, 2, \dots, N_{\text{zed}} \text{ with } i_1 < i_2 < \dots < i_n, \\ &\dots && \end{aligned} \quad (21)$$

Summing all contributions, we obtain

$$\langle |q| \rangle = 1 - \frac{2}{2^{N_{\text{zed}}} L^d} \left[\sum_i v_i + \sum_{i < j} (v_i + v_j) + \dots \right] = 1 - \alpha_{\text{zed}}, \quad (22)$$

where

$$\alpha_{\text{zed}}(L) \equiv \frac{1}{L^d} \sum_{i=1}^{N_{\text{zed}}} v_i = \int_1^{L^d/2} v n_{\text{zed}}(v) dv. \quad (23)$$

We can now compute $\langle q^2 \rangle$ in the same way. We obtain

$$\langle q^2 \rangle = \frac{1}{2^{N_{\text{zed}}}} \left[\sum_i \left\{ 1 - \frac{2}{L^d} v_i \right\}^2 + \sum_{i < j} \left\{ 1 - \frac{2}{L^d} (v_i + v_j) \right\}^2 + \dots \right]. \quad (24)$$

which reduces to

$$\langle q^2 \rangle = (1 - \alpha_{\text{zed}})^2 + \beta_{\text{zed}}, \quad (25)$$

or

$$\langle q^2 \rangle - \langle |q| \rangle^2 = \beta_{\text{zed}}, \quad (26)$$

where

$$\beta_{\text{zed}}(L) \equiv \frac{1}{L^{2d}} \sum_{i=1}^{N_{\text{zed}}} v_i^2 = \frac{1}{L^d} \int_1^{L^{d/2}} v^2 n_{\text{zed}}(v) dv. \quad (27)$$

Similarly we have

$$\langle q^4 \rangle - 3\langle q^2 \rangle^2 + 2\langle |q| \rangle^4 = -2\gamma_{\text{zed}}, \quad (28)$$

where

$$\gamma_{\text{zed}}(L) \equiv \frac{1}{L^{4d}} \sum_{i=1}^{N_{\text{zed}}} v_i^4 = \frac{1}{L^{3d}} \int_1^{L^{d/2}} v^4 n_{\text{zed}}(v) dv. \quad (29)$$

If the droplet picture is correct, the order-parameter distribution $P(q)$ has only two delta-function peaks at the $L \rightarrow \infty$ limit. Then in this limit both the left-hand side of Eq. (26) and that of Eq. (28) vanish. This condition is satisfied if the density distribution of the zero-energy droplets $n_{\text{zed}}(v)$ decays fast enough as $v \rightarrow \infty$. If $n_{\text{zed}}(v)$ decays exponentially, the integrals in Eqs. (27) and (29) give finite values; hence $\beta_{\text{zed}}(L) = O(L^{-d})$ and $\gamma_{\text{zed}}(L) = O(L^{-3d})$. If $n_{\text{zed}}(v)$ decays as v^{-x} with $x > 2$, we have $\beta_{\text{zed}}(L) = O(L^{-d \min(1, x-2)})$ and $\gamma_{\text{zed}}(L) = O(L^{-d \min(3, x-2)})$.

On the other hand, if the mean-field picture is correct, the order-parameter distribution $P(q)$ has a non-trivial part as $L \rightarrow \infty$. In this case, $\alpha_{\text{zed}}(L)$, $\beta_{\text{zed}}(L)$, and $\gamma_{\text{zed}}(L)$ all give finite values as $L \rightarrow \infty$. These conditions are satisfied if the distribution function decays as $n_{\text{zed}}(v) \sim v^{-2}$.

In our numerical results, both $\beta_{\text{zed}}(L)$ and $\gamma_{\text{zed}}(L)$ appear to be decreasing as L is increased (Fig. 14). The decrease is roughly $O(L^{-1})$, although the statistical errors are too large to make a more definite statement. This behavior is additional evidence for the droplet picture. From our numerical results we suggest that the size distribution of the zero-energy droplets decays as $n_{\text{zed}}(v) \sim v^{-x}$ with $x > 2$.

IV. SUMMARY

As we have illustrated, the results of our multicanonical Monte Carlo calculation suggest the droplet picture in contrast to most previous Monte Carlo simulations of the three-dimensional random bond Ising model. Our main findings supporting the droplet picture are (1) $P(q)$ near $q \simeq 0$ decreasing at low temperatures as the system size is increased, (2) the Binder parameter approaching unity at low temperatures, and (3) the effect of the ground-state degeneracy on moments of the overlap order parameter.

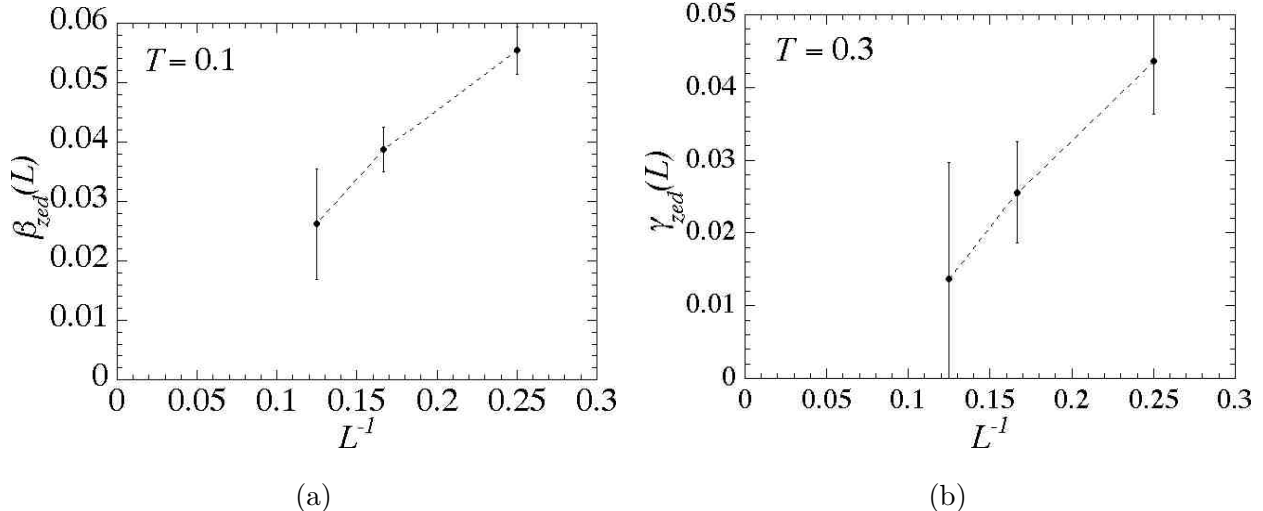


FIG. 14: The size dependence of (a) $\beta_{zed}(L)$ and (b) $\gamma_{zed}(L)$. Both quantities are vanishing as $L \rightarrow \infty$.

Our disagreement with previous Monte Carlo simulations may be understood if there are many local free-energy minima with small q , the simulations become trapped by them, causing one to overestimate $P(q)$ near $q = 0$, particularly when the system size is increased. This scenario is supported by a recent study by Sandvik [30] where a series of simulated annealing calculations were performed with different annealing rates and estimates of $P(q)$ were made after each annealing. Sandvik showed that the ground-state estimate of $P(0)$ is greater for faster annealing than for slower annealing (which should be more precise). His results suggest that simulations without substantial equilibration overestimate $P(0)$. Others have also noted that low temperature data agrees with the droplet picture [31].

After the publication of our preliminary results [3], Hartmann [15] published the same conclusion for the order-parameter distribution of the ground states.

Acknowledgments

We gratefully acknowledge computational support from the Applied Mathematics program of the Department of Energy for the use of the massively parallel computers at NERSC, from the Center for Nonlinear Studies (CNLS) at Los Alamos National Laboratory for the use of its parallel computer Avalon, and from the Los Alamos Directed Research program at Los Alamos for computer time on the ASCI Blue Mountain computer. The use of the random-number generator library SPRNG of National Center for Supercomputing Appli-

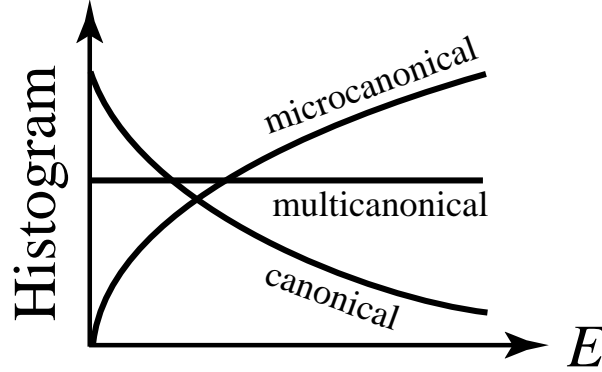


FIG. 15: Schematic of the histograms of energy values generated in the micro-canonical, canonical, and multicanonical simulations.

cations (NCSA) at University of Illinois is also gratefully acknowledged. A part of the computation was also carried out on a PC-cluster parallel computer ARK of Aoyama Gakuin University [32].

APPENDIX A: MULTICANONICAL MONTE CARLO METHOD

In this Appendix, we describe the multicanonical Monte Carlo method from a viewpoint [4] slightly different from other authors [24, 25, 26, 27, 28]. We first compare it with micro-canonical and canonical methods.

Suppose that we simulate with the importance weight $W(E)$ and histogram the energy E values. After equilibration of the simulation, each microscopic state (spin configuration) is generated at a rate proportional to $W(E)$. The rate at which a thermodynamic state with the energy E appears is proportional to $D(E)W(E)$, where $D(E)$ is the density of states.

In the micro-canonical (or very naive) simulation, we generate all microscopic states at the same rate. In other words, we set $W(E) = \text{const.}$, and hence the resulting histogram is proportional to the density of states: $h(E) \propto D(E)$ (see Fig. 15). In many cases, the density of states becomes very small in low-energy regions. Hence simulations based on the micro-canonical ensemble are generally not suitable for investigating low-temperature properties because the low-energy states that dominate the thermodynamic average at low temperatures are generated only infrequently, if at all.

Importance sampling algorithms, like the Metropolis algorithm for canonical ensemble,

were developed to overcome this difficulty. Here states are generated with the importance weight $W(E) \propto e^{-\beta E}$, and hence the energy histogram is $h(E) \propto e^{-\beta E} D(E)$. Thus, in ideal cases, low-energy states appear at a greater frequency at low temperatures. In spin-glass simulations, however, the simulation tends to get stuck in local minima of the free-energy landscape.

In the multicanonical simulations, the importance weight is set to $W(E) \propto 1/D(E)$, and hence the energy histogram should be flat. (Of course, we cannot set $W(E) \propto 1/D(E)$ because we do not know the density of states *a priori*. However, the multicanonical method is a procedure that makes the importance weight converge to the reciprocal of the density of states [33].) The aim is to ensure better statistics of low-energy states than in the microcanonical method and, at the same time, generate more high-energy states than in the canonical method so that the system can escape local free-energy minima.

Berg and others have invented [24, 25] and applied [26, 27, 28] this method to spin glasses, taking the weight of each spin configuration $\{\sigma\}$ either as

$$W(\{\sigma\}) \propto 1 / D(E(\{\sigma\})) \quad (\text{A1})$$

or

$$W(\{\sigma\}) \propto 1 / D(q(\{\sigma\})), \quad (\text{A2})$$

where $D(E)$ is the density of states with respect to the energy and $D(q)$ is the one with respect to the overlap order parameter. It has been argued [34] that “simulated tempering [35],” where replicas at different temperatures have an equal weight, is mathematically similar to taking the weight (A1).

In the ideal situation, the multicanonical simulation effectively generates a random walk in the macroscopic phase space, because all the thermodynamic states should appear with the same probability. We can deduce from this that the autocorrelation time of the thermodynamic variable (E in the above case) is proportional to the volume (the number of the sites). In the simulation of the $\pm J$ model, the energy change after each spin flip is of the order of J . On the other hand, the upper and lower bounds of the energy are of the order of NJ , where $N = L^d$ is the number of the spins. Hence the number of spin flips necessary for the random walk to cover the entire energy phase space is of the order of N^2 . Thus if random walk is in energy space, a one-dimensional space, the measured energy should decorrelate after N^2 Monte Carlo steps or N Monte Carlo sweeps.

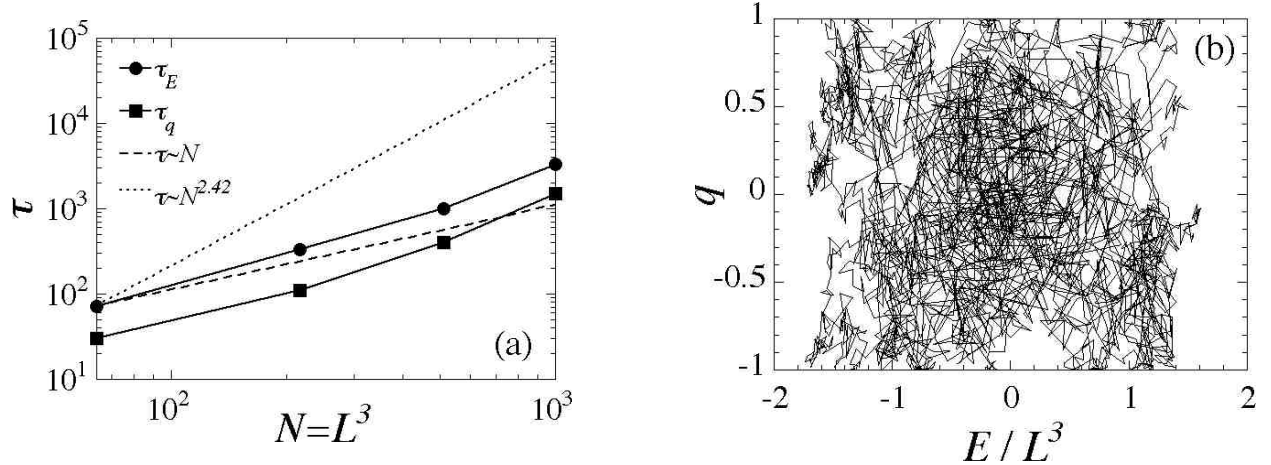


FIG. 16: (a) System-size dependence of the autocorrelation time τ with respect to E and q . The dotted line represents the power law $\tau \propto N^{2.42}$, which was reported in [28]. (b) An example of the random walk in the phase space (E, q) . The system size simulated here is $L = 4$. The time series of 2500 Monte Carlo sweeps after equilibration is plotted.

This ideal situation was not achieved in the previous applications of the multicanonical simulations to spin glasses [26, 27, 28]. Berg *et al.* reported $\tau \propto N^{2.8}$ for the importance weight (A1) [26] and $\tau \propto N^{2.42}$ for the importance weight (A2) [28]. (Here τ is measured in the unit of Monte Carlo *sweep*.) This suggests that the slow dynamics in the low-energy region was not removed completely in these mono-variate multicanonical simulations. (Note, however, that Berg *et al.* did not use the conventional definition of the autocorrelation time in measurement of τ . This might be a contribution to the above power law behavior.)

In the present study, we carried out the simulation using the bivariate importance weight:

$$W \propto 1 / D(E, q). \quad (\text{A3})$$

As shown in Fig. 16 (a), we almost achieved the ideal situation $\tau \propto N$. The random walk in the two-dimensional phase space is illustrated in Fig. 16 (b).

There is a drawback with the bivariate simulation: large memory is needed to store the data from which the bivariate histogram is constructed. The number of bins in the energy phase space is of the order of L^d and is similarly sized in the q phase space. Hence an array of the size L^{2d} is necessary to store each density of states $D(E, q)$, the histogram $h(E, q)$, and related work space. The combined storage requirements amounted to nearly 30MB per sample for $L = 10$ and 400MB per sample for $L = 16$. Based on direct comparisons with the original mono-variate multicanonical method, we have however concluded that the use

of both E and q for spin-glass simulations is essential for improving the slow dynamics [3]. We comment that bivariate multicanonical Monte methods have been previously used in different contexts, *e.g.*, protein folding simulations [36, 37].

The actual algorithm of the multicanonical method has the following structure:

- (A) Make a guess at the density of states, $D_0(E, q)$. Start the following loop with $i = 0$.
- (B) The outer loop (multicanonical-iteration loop):
 - (a) Set the importance weight to $W_i = 1/D_i$. Calculate the energy and the order parameter of the initial spin configuration, E_0 and q_0 . Start the following loop with $j = 0$.
 - (b) The inner loop (spin-update loop):
 - (i) Choose a spin to be updated. Calculate the energy and the order parameter, E'_j and q'_j , assuming that the spin is actually flipped.
 - (ii) Calculate the spin-flip probability as
$$P_{\text{flip}} = \min \left(1, \frac{W_i(E'_j, q'_j)}{W_i(E_j, q_j)} \right) \quad (\text{A4})$$
 - (iii) Draw a random number $R \in [0, 1]$. If $R < P_{\text{flip}}$, flip the spin and make the substitution $E_{j+1} = E'_j$ and $q_{j+1} = q'_j$. Otherwise, keep the current spin configuration and make the substitution $E_{j+1} = E_j$ and $q_{j+1} = q_j$.
 - (iv) Increment the histogram bin $h_i(E_{j+1}, q_{j+1})$ by one.
 - (v) Increment the number of steps j by one and go to the step (i) until j exceeds a pre-determined number.
 - (c) Measure physical quantities $Q(E, q)$ via

$$\langle Q \rangle_i = \frac{1}{Z_i} \sum_{E, q} Q(E, q) e^{-\beta E} h_i(E, q) D_i(E, q), \quad (\text{A5})$$

where the partition-function estimate is given by

$$Z_i = \sum_{E, q} e^{-\beta E} h_i(E, q) D_i(E, q). \quad (\text{A6})$$

- (d) Update the guess of the density of states as follows: [33]

$$D_{i+1}(E, q) = \frac{D_i(E, q) (h_i(E, q) + 1)}{\text{Normalizaion}}. \quad (\text{A7})$$

The normalization constant is chosen so that the integration of the density of states becomes unity. (An extra count is added to the histogram in (A7) in order to avoid zero division in setting the next importance weight $W_{i+1} = 1/D_{i+1}$ [33].)

- (e) Increment the number of multicanonical iterations i by one and go to the step (a), until the histogram meets certain conditions of being flat.

The step (iv) should be skipped until the simulation reaches “equilibrium” for the importance weight W_i . In our simulation, the number of equilibration Monte Carlo sweeps were a few times longer than the number of sweeps measured by the autocorrelation time.

It is also best to skip the step (c) until the histogram h_i becomes practically flat. In principle, the estimator (A5) should be applicable even before the histogram becomes flat. With sufficient statistics, the histogram h_i would be proportional to $W_i(E, q)D(E, q) = D(E, q)/D_i(E, q)$, where $D(E, q)$ is the true density of states. Thus the estimator (A5) would give

$$\langle Q \rangle_i \simeq \frac{1}{Z_i} \sum_{E, q} Q(E, q) e^{-\beta E} D(E, q), \quad (\text{A8})$$

with the partition function

$$Z = \sum_{E, q} e^{-\beta E} D(E, q). \quad (\text{A9})$$

In practice, however, a limited number of Monte Carlo steps can cause large errors wherever h_i is small.

During convergence, the histogram at first is typically concentrated in the mid-part of the density of states and expands outward towards the upper and lower bounds of the energy until it becomes flat. We defined the histogram to be flat, whenever the bin count at the center of the density of states and at the edges of the density of states approximately equaled the average histogram count.

We repeated the outer loop five times after we determined that the histogram became flat so that we could detect erroneous estimates of the density of states. We also divided the inner loop into a few sections, from which we calculated the statistical errors. Errors at different temperatures of the same random bond configuration are generally correlated in multicanonical simulations.

We comment that all physical quantities could have been calculated after all the simulations were completed, provided we had stored the density of states for each random bond

configuration on disk. This procedure would require a huge disk because of the need to simulate a large number of random samples.

-
- [1] S. F. Edwards and P. W. Anderson, J. Phys. F: Metal Phys. **5**, 965–974 (1975).
 - [2] K. Binder and A. P. Young, Rev. Mod. Phys. **58**, 801–976 (1986).
 - [3] Preliminary results have been reported at the 8th Tohwa University International Symposium, Fukuoka, Japan, at the 12th Annual Workshop of Center for Simulation Physics, University of Georgia, and at the 5th International Conference on Computational Physics, Kanazawa, Japan. See the proceedings, N. Hatano and J. E. Gubernatis, in *Slow Dynamics in Complex Systems*, edited by M. Tokuyama and I. Oppenheim, pp. 565–566 (American Institute of Physics, Maryland, 1999); in *Recent Developments in Computer Simulation Studies in Condensed Matter Physics*, edited by D. P. Landau, pp. 149–161 (Springer, Berlin, 2000); Prog. Theor. Phys. Suppl. **138** 442–447 (2000).
 - [4] J. Gubernatis and N. Hatano, Computing in Science & Engineering **2**, No.2, 95–102 (2000).
 - [5] D. S. Fisher and D. A. Huse, Phys. Rev. Lett. **56**, 1601–1604 (1986).
 - [6] D. S. Fisher and D. A. Huse, Phys. Rev. B **38**, 386–411 (1988).
 - [7] N. Kawashima and A. P. Young, Phys. Rev. B **53**, R484–R487 (1996).
 - [8] K. Hukushima, H. Takayama and K. Nemoto, Int. J. Mod. Phys. C **7**, 337–344 (1996).
 - [9] For a review, M. Mézard, G. Parisi and M. Virasoro, *Spin Glass Theory and Beyond* (World Scientific, Singapore, 1987).
 - [10] D. Sherrington and S. Kirkpatrick, Phys. Rev. Lett. **35**, 1792–1796 (1975).
 - [11] G. Parisi, Phys. Rev. Lett. **43**, 1754–1756 (1979).
 - [12] E. Marinari, G. Parisi, J. Ruiz-Lorenzo and F. Ritort, Phys. Rev. Lett. **76**, 843–846 (1996).
 - [13] D. Iñiguez, E. Marinari, G. Parisi and J. Ruiz-Lorenzo, J. Phys. A: Math. Gen. **30**, 7337–7347 (1997).
 - [14] E. Marinari, Phys. Rev. Lett. **82**, 434–437 (1999).
 - [15] A. Hartmann, cond-mat/9906270, to be published in Euro. J. Phys.
 - [16] M. Palassini and A. P. Young, cond-mat/9906323, cond-mat/9910278, and cond-mat/0002134.
 - [17] T. Komora, H. Yoshino, and H. Takayama, cond-mat/9904143 and cond-mat/9908078.
 - [18] C. M. Newman and D. L. Stein, Phys. Rev. Lett. **76**, 515–518 (1996).

- [19] C. M. Newman and D. L. Stein, Phys. Rev. E **57**, 1356–1366 (1998).
- [20] M. A. Moore, H. Bokil and B. Drossel, Phys. Rev. Lett. **81**, 4252–4255 (1998).
- [21] E. Marinari, G. Parisi, J. J. Ruiz-Lorenzo, and F. Zuliani, cond-mat/981234.
- [22] H. Bokil, A. J. Bray, B. Drossel, and M. A. Moore, cond-mat/9902068.
- [23] W. Wu, B. Ellman, T. F. Rosenbaum, G. Aeppli and D. H. Reich, Phys. Rev. Lett. **67**, 2076–2079 (1991).
- [24] B. Berg and T. Neuhaus, Phys. Lett. B **267**, 249–253 (1991).
- [25] B. Berg and T. Neuhaus, Phys. Rev. Lett. **68**, 9–12 (1992).
- [26] B. A. Berg, U. Hansmann and T. Celik, Phys. Rev. B **50**, 16444–16452 (1994).
- [27] B. A. Berg, J. Stat. Phys. **82**, 323–342 (1996).
- [28] B. A. Berg and W. Janke, Phys. Rev. Lett. **80**, 4771–4774 (1998).
- [29] For example, A. K. Hartmann, Ground-state entropy of three-dimensional $\pm J$ Ising spin glasses via ballistic search, cond-mat/9902120.
- [30] A. Sandvik, Europhys. Lett., **45**, 745–746 (1999).
- [31] M. A. Moore, H. Bokil, and B. Drossel, cond-mat/9808140; B. Drossel, Bokil, M. A. Moore, and A. J. Bray, cond-mat/9905354.
- [32] H. Nataka, N. Hatano, N. Furukawa and K. Kubo, Prog. Theor. Phys. Suppl. **138**, 757–758 (2000).
- [33] G. R. Smith and A. D. Bruce, J. Phys. A: Math. Gen. **28**, 6623–6643 (1995).
- [34] U. Hansmann and Y. Okamoto, Tempering. Phys. Rev. E **54**, 5863–5865 (1996).
- [35] E. Marinari and G. Parisi, Europhys. Lett. **19**, 451–458 (1992).
- [36] J. Higo, N. Nakajima, H. Shirai, A. Kidera and H. Nakamura, J. Comp. Chem. **16**, 2086–2092 (1997).
- [37] Y. Iba, G. Chikenji and M. Kikuchi, J. Phys. Soc. Jpn. **67**, 3327–3330 (1998).